Surface Science 516 (2002) 179–190

SURFACE SCIENCE

www.elsevier.com/locate/susc

STM and STS study of ultrathin Mn layers on Fe(0 0 1)

T.K. Yamada [a,b], M.M.J. Bischoff [a], T. Mizoguchi [b], H. van Kempen [a,*]

[a] *NSRIM, University of Nijmegen, Toernooiveld 1, 6525 ED Nijmegen, The Netherlands*
[b] *Faculty of Science, Gakushuin University, 171-8588 Mejiro, Tokyo, Japan*

Received 4 May 2002; accepted for publication 21 June 2002

Abstract

The growth of ultrathin Mn films on an Fe(0 0 1) whisker at 370 K is studied by scanning tunneling microscopy (STM) and scanning tunneling spectroscopy at room temperature in ultrahigh vacuum. Atomically and chemically resolved STM images show that the Mn film grows with the same in-plane lattice constant as Fe(0 0 1) and that Fe atoms intermix with the first (14%), the second (4%), and the third Mn layer (2%), while a negligible amount of Fe atoms is found above the third layer. The growth mode changes from layer-by-layer to layer-plus-island at a coverage of 3 ML Mn. dI/dV curves which are normalized by voltage-dependent tunneling probability functions show clear peaks on each Mn layer. These peaks are tentatively ascribed to surface states. On the first Mn layer, peaks are found at +0.35 eV on pure Mn areas and at +0.28 eV on mixed MnFe areas. The second and the third Mn layer show peaks at +0.20 and +0.8 eV, respectively. Mn films thicker than three layers reveal besides a strong peak at +0.8 eV a weaker peak at −0.6 eV. Our apparent step height measurements show that the Mn film relaxes at the third layer: the interlayer spacing is ~0.16 nm for the first two layers, and it increases to ~0.18 nm at the third layer. Starting from the fourth layer the interlayer spacings are geometrically equivalent (~0.165 nm).

Keywords: Epitaxy; Iron; Magnetic films; Manganese; Scanning tunneling microscopy; Scanning tunneling spectroscopies; Surface structure, morphology, roughness, and topography; Whiskers

---

1. Introduction

The development of epitaxial growth techniques has led to considerable practical applications such as metallic-multilayers devices. Especially, ultrathin magnetic films evaporated on magnetic substrates show enormous different magnetic and electronic properties compared to the bulk caused by their lower dimensions ([1] and references therein). Regarding the novel magnetic and electronic properties at the surface and the interface, particularly, the system of Mn films on Fe(0 0 1) is remarkable since recent calculations [2–13] and experiments [14–27] show conflicting results indicating the complicated relation between growth condition, electronic structure, and magnetic coupling.

With reflective high energy electron diffraction, quantitative low energy electron diffraction (LEED), and extended X-ray absorption spectroscopy (EXAFS), it has been shown that Mn

---

[*] Corresponding author. Tel.: +31-24-3653499; fax: +31-24-3652190.

E-mail address: hvk@sci.kun.nl (H. van Kempen).

0039-6028/02/$ - see front matter © 2002 Elsevier Science B.V. All rights reserved.
PII: S0039-6028(02)02032-0

layers grow layer-by-layer on Fe(0 0 1) up to more than 10 monolayers (MLs). The in-plane lattice constant is 0.287 nm and interlayer spacings of 0.130 [24] or 0.148 nm [25] for 1 ML, 0.152 nm [25] for 2 ML, and 0.161 nm [24] or 0.164 nm [26] for 14–25 ML are reported, i.e., the structure is body-centered-tetragonal (bct). These results have been reported for Mn growth on an Fe(0 0 1)-single-crystal at room temperature (RT) [24], on Fe(0 0 1)-films/MgO(0 0 1) at RT [25], and on an Fe(0 0 1) whisker at 320 K [26]. Auger electron spectroscopy and grazing ion-surface scattering measurements showed that a layer-by-layer Mn film changes to a layer-plus-island Mn film when a 13 ML thick Mn film, which is deposited at RT on an Fe(0 0 1)-single-crystal, is annealed at 420 K [15].

Nonas et al. showed with a Korringa, Kohn, and Rostoker Green's function method calculation that for Mn atoms on Fe(0 0 1) it is energetically favorable to place exchange with the Fe surface atoms [3,4]. Bischoff et al. showed with chemically resolved scanning tunneling microscopy (STM) and scanning tunneling spectroscopy (STS) the formation of a surface alloy for submonolayer Mn films grown on Fe(0 0 1) at substrate temperatures above 370 K [28]. Grazing ion-scattering experiments showed that Fe atoms intermix with Mn adlayers up to a coverage of 3 ML at a substrate temperature of 420 K [16].

In this paper, a study on the atomic morphology by STM and the electronic structure by STS is reported for Mn films grown on an Fe(0 0 1) whisker at 370 K. Growth at this temperature is believed to lead to reasonable flat films [17] and low intermixing [28]. With special tip conditions a high chemical contrast can be achieved which is utilized in determining the intermixing behavior.

2. Experimental

STM and STS measurements were performed in ultrahigh vacuum (UHV) ($\sim 5 \times 10^{-11}$ mbar) at RT with a commercial STM (Omicron UHV STM-1). For getting a sharp STM tip, a W polycrystalline wire with a diameter of 0.5 mm (purity 99.99%) was etched with a 5 M KOH solution and subsequently rinsed with ethanol in air. In UHV, the tip was heated up to 1000 K and self-sputtered with Ar or Ne in order to clean the tip and to decrease its radius below 10 nm as verified by field-emission spectroscopy [29]. To obtain a clean and flat substrate surface an Fe(0 0 1) whisker was used in this study [30]. Using Ar sputtering (750 eV) cycles at 1020 K, the Fe(0 0 1) whisker, with dimensions $7 \times 0.5 \times 0.5$ mm^3, was cleaned until the concentration of surface contaminants became lower than 1% as measured by Auger spectroscopy and atomically resolved STM images. Mn (purity 99.999%) was sublimated from a Knudsen cell at a deposition rate of ~0.3 ML/min as estimated by a quartz crystal oscillator. Here, one ML is defined as one Mn atom per Fe atom on the (0 0 1) surface. In the present paper, the local Mn coverage is obtained from a Gaussian fit to the distribution of exposed layers (see Fig. 2a). During the growth, the pressure was always around 4×10^{-10} mbar. The substrate was radiatively heated to 370 K. It must be noted that the inaccuracy of the temperature measurements is estimated to be ±20 K at 370 K since the thermocouple was not in direct contact with the sample. Using the Fe single step height of bcc-Fe(0 0 1) which is 0.143 nm, the apparent step heights of our STM measurements were calibrated. STS measurements were performed by recording an $I(V)$ curve at every pixel of a topographic scan which is obtained at the typical setpoint of $V_S = -0.5$ V, $I = 0.5$ nA. dI/dV curves were obtained by numerical differentiation of the $I(V)$ curves.

3. Results and discussion

3.1. The growth of Mn layers on Fe(0 0 1)

Monoatomic steps can be observed with an interval of about 200 nm at the clean Fe(0 0 1) whisker substrate (Fig. 1a). When 1.5 ML Mn is deposited at a substrate temperature of 370 K, Mn grows layer-by-layer. This follows from Fig. 1b in which it can be seen that the second layer islands have started to grow after the first layer has been completed. At a coverage of 3 ML, the second, the

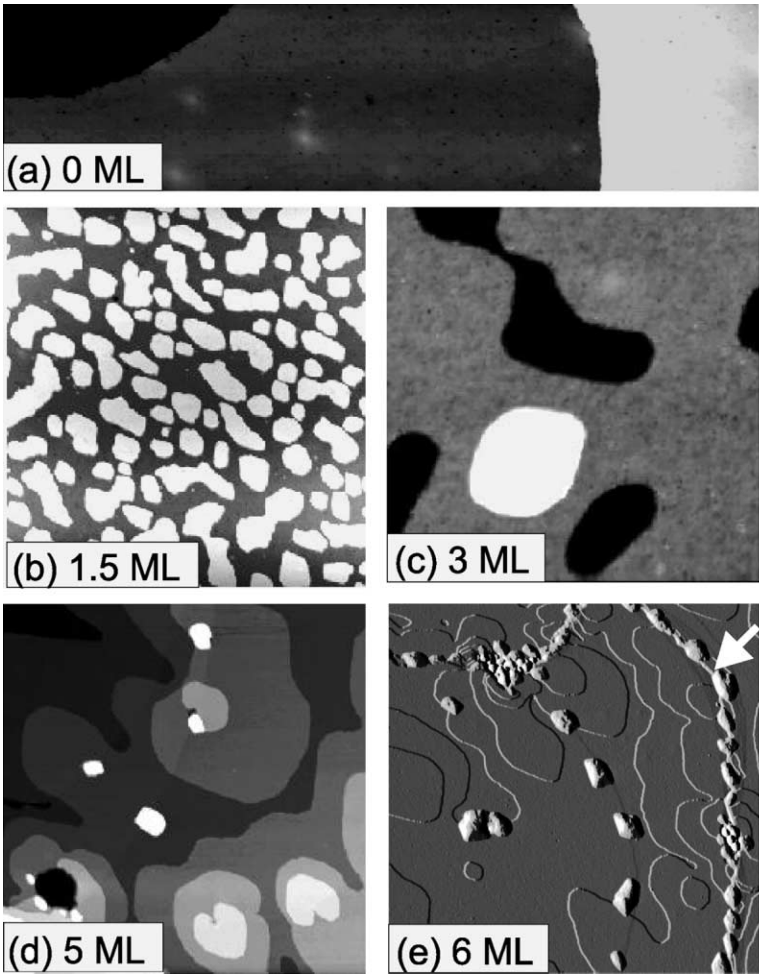

Fig. 1. STM topographic images of Mn layers grown on the Fe(0 0 1) whisker at 370 K. (a) The bare whisker, 310 × 80 nm^2, $V_S = -1.00$ V, $I = 0.06$ nA; (b) 1.5 ML, 165 × 157 nm^2, $V_S = -0.38$ V, $I = 0.05$ nA; (c) 3 ML, 100 × 100 nm^2, $V_S = -0.34$ V, $I = 2.00$ nA. The second, third, and fourth layer are visible. (d) 5 ML, 200 × 200 nm^2, $V_S = -1.00$ V, $I = 0.05$ nA; (e) 6 ML, 300 × 300 nm^2, $V_S = -1.00$ V, $I = 0.05$ nA. (e) shows the data in the differential mode in which the grey scale is proportional to the gradient of the height variation along each scan line.

third, and the fourth layer are observed as trenches, terrace, and islands, respectively (Fig. 1c). Before the second layer has been completely covered by Mn, the fourth layer has started to grow which means that the growth mode is not layer-by-layer anymore. At coverages above 3 ML, the appearance of the surface changes drastically and many levels are exposed on the surface (Fig. 1d). Whereas, up to a coverage of 6.5 ML Mn, hidden Fe steps are clearly observed on the Mn(0 0 1) surface as about 0.02 nm high steps, the Fe step height of 0.143 nm is never observed, which means that the overlaying Mn film tends to make the surface flat. Three dimensional (3D) islands (~5 nm high) are observed at the position of hidden Fe steps and defects marked by the white arrow in Fig. 1e. This figure is displayed in the differential mode and shows that the islands have pyramid-like shapes which corresponds to the results reported by Pfandzelter et al. [15].

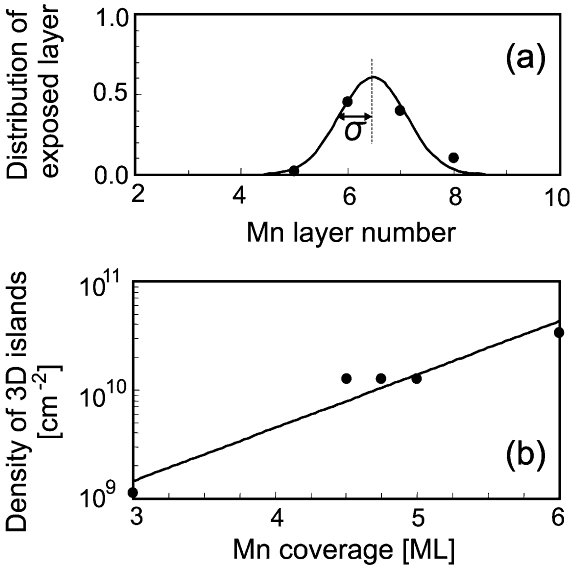

Fig. 2. (a) Distribution of exposed Mn layers at a coverage of 6.5 ML Mn. Average Mn coverage and its deviation, σ, are obtained from a Gaussian fit and (b) the dependence of the 3D islands density on Mn coverage. The 3D islands appear at a coverage of 3 ML and their density increases with the coverage. The solid line is a guide to the eye.

Pierce et al. found that the distribution of the exposed layers can be approximated by a Gaussian. The center of the Gaussian gives the average coverage, and the deviation σ the root-mean-square height variation or roughness [14,31]. Thus, σ can be obtained from our STM images (Fig. 2a). σ is 0.40 ± 0.05 and 0.7 ± 0.1 ML for coverages below and above 3 ML Mn, respectively. If the layer-by-layer growth continued for coverages above 3 ML, we do not expect an increase of σ. However, σ drastically increases by a factor of two at coverages above 3 ML in our experiments, which is a clear indication that the growth mode changes. Furthermore, starting from around a coverage of 3 ML Mn, the number of 3D islands strongly increases as can be observed in Fig. 2b. The density of the 3D islands at a coverage of around 5 ML Mn ($\sim 10^{10}$ cm^{-2}) corresponds with the results reported by Pfandzelter et al. [15]. Based upon both the increase of σ and the appearance of 3D islands, the critical coverage where the growth mode changes from layer-by-layer to layer-plus-island is estimated to occur around 3 ML.

The layer-plus-island growth can be understood by equilibrium thermodynamics [15,32,33] which state for the Mn/Fe system that if $\Delta\gamma = \gamma_{\mathrm{Mn}} + \gamma_{\mathrm{in}} + \gamma_{\mathrm{s}} - \gamma_{\mathrm{Fe}}$ is negative (positive), the layers grow layer-by-layer (layer-plus-island). γ_{Mn} and γ_{Fe} are surface energies of Mn and Fe, respectively. γ_{in} is the interface energy and γ_{s} is the strain energy. The Fe surface energy ($\sim$2.6 J/m^2) is higher than the Mn surface energy ($\sim$1.6 J/m^2) [34] and the interfacial energy is assumed to be much smaller than the surface energy [15]. The strain energy is caused by the lattice mismatch. The lattice mismatch between Fe and Mn is difficult to determine since a stable bulk bcc or fcc structure does not exist at RT and consequently lattice parameters for the bcc and fcc structures must be extrapolated from either high temperature phases or alloyed phases [24]. Kim et al. showed that the observed bct structure of Mn films might be a distortion of either a fcc or a bcc phase. Based upon their analysis the in-plane lattice mismatches are estimated −8% and +4% for fcc and bcc, respectively [24]. Due to this high lattice mismatch the strain energy plays a key role for the change of the growth mode. In our case, due to an increase of the strain energy, the total energy $\Delta\gamma$ is likely to change from negative to positive at a coverage of 3 ML and consequently layer-plus-island growth sets in.

Our STM topographic results differ from the results reported by Tulchinsky et al. which showed that for comparable growth rate and temperature the layer-by-layer growth continues up to 10 ML without any 3D islands [14,17]. The Fe whisker used in this study is not of the high flatness (see Fig. 1a) as the ones used by Tulchinsky et al. [17], i.e., our Fe whisker has a higher Fe step density. Furthermore, various defects can be observed on the Fe(0 0 1) surface [35], e.g., "Ar bubble-like" defects [36,37], holes ($\sim$5 nm deep) caused by the sputtering, and screw dislocations. Since this non-ideal surface morphology is expected to lead to an increase of the interface energy, an influence on the growth process is likely. Therefore, the onset seems to depend strongly on the quality of the Fe(0 0 1) whisker although it may depend on the growth rate and temperature as well.

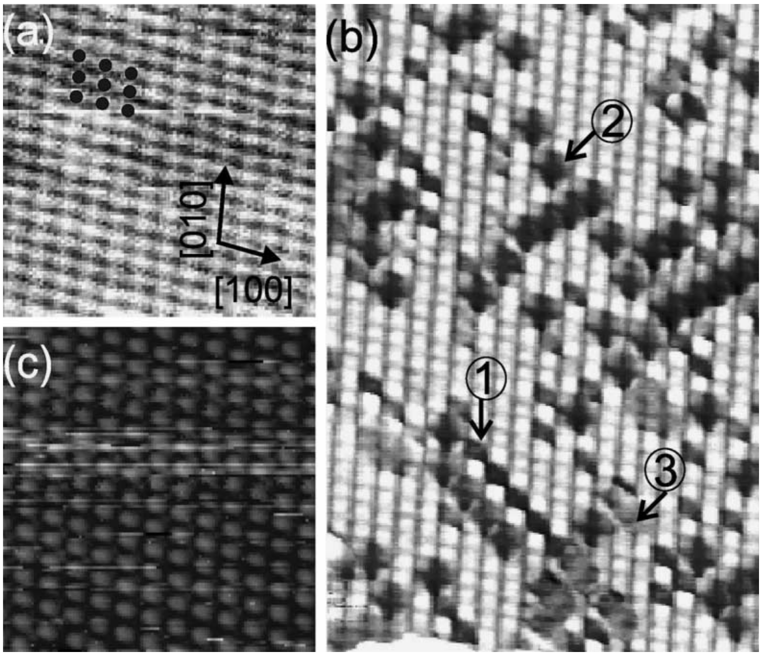

Fig. 3. Atomically and chemically resolved STM images of (a) the Fe(0 0 1) substrate (3.5 × 3.5 nm^2, $V_S = -2$ mV, $I = 2.3$ nA), (b) the first (6 × 9 nm^2, $V_S = -2$ mV, $I = 2.6$ nA), and (c) the fifth Mn layer (3.5 × 3.5 nm^2, $V_S = -7$ mV, $I = 2.6$ nA), respectively. The black dots in (a) indicate the positions of the atoms. The close-packed directions are shown in (a). Numbers in (b) denote three kinds of depressions on the surface (see text). The images are slightly distorted by thermal drift (~0.3 nm/min). The in-plane lattice constant along the [1 0 0] and [0 1 0] directions in the Mn layer is the same as the lattice constant of Fe(0 0 1).

3.2. Atomically and chemically resolved STM topographic images

Fig. 3 shows atomically resolved STM topographic images obtained on the Fe(0 0 1) substrate (a), the first (b), and the fifth (c) Mn adlayer, respectively. Atomically resolved images could be observed on all Mn adlayers studied (i.e., up to the seventh Mn layer). The STM images include a slight distortion due to thermal drift (~0.3 nm/min) resulting in a deviation from 90° of the angle between the close-packed lattice directions (which are indicated in Fig. 3a) [28]. From the atomically resolved STM images it can be concluded that for all the Mn adlayers the in-plane lattice constant equals the Fe(0 0 1) lattice constant within the accuracy of STM, which corresponds with the results of quantitative LEED [24]. Furthermore, since there is no indication for an in-plane relaxation such as dislocation networks, the Mn adlayer must follow the Fe substrate lattice.

With a normal tip condition [1] the corrugation of the lattice atoms is about 1 pm which is of the order of the noise level of our STM. Consequently, the atoms can hardly be observed in the topographic image. Fortunately, occasionally special tip conditions could be obtained during STM measurements, e.g., the corrugation of the Fe atoms increases to more than 10 pm as shown in Fig. 3a. With this tip condition, the corrugation of the Mn lattice atoms increases to 35 pm and atomically resolved images could be obtained with high chemical contrast (Fig. 3b).

The chemically resolved image obtained on the first Mn layer shows three kinds of depressions. The depressions marked “1” (~60 pm deep) and marked “2” (~60 pm deep) are observed at lattice

---

[1] A normal tip condition is defined as a tip which does not show chemical contrast. Normal refers to the higher chance of having this kind of tip compared to a tip leading to chemical contrast.

sites and hollow sites, respectively. The concentration of both depressions is the same, i.e., 7 ± 1%. In Fig. 3b, depressions marked "3" are observed as well. Their concentration is much lower (~1%) and their contrast is much weaker (~25 pm deep).

To identify these three kinds of depressions, the possibility of oxidation must be considered. Mn atoms are easily oxidized to MnO [27]. Andrieu et al. proposed that the main cause of the oxidation of the Mn layer is CO dissociation which is already effective at RT on Mn ([27] and references therein). In their experimental setup, the oxidation speed of the Mn layer was 0.03 ML/h from which a CO partial pressure of 2.5×10^{-11} Torr was estimated. Using mass spectrometry, the CO partial pressure in our STM chamber is estimated to be about 10 times better, which implies that the oxidation speed in our system is below 0.003 ML/h. Our atomically resolved STM images were measured about 5 h after the Mn layers had been grown, which implies that the total amount of oxygen contamination is below 1.5%. Furthermore, with Auger spectroscopy, the concentration of impurities (mainly oxygen) on our Fe(0 0 1) whisker is estimated to be 1% which is about the detection limit of our Auger setup.

Since the concentration of the atoms marked "1" and "2" is much higher than the impurity concentration, these depressions are not likely to be contaminants but rather the effect of intermixed Fe atoms. The two types of depressions are tentatively explained by different local environments of the Fe atoms: i.e., having 4 Fe nearest neighbors or 3 Fe and 1 Mn nearest neighbors in the layer below. Calculations and experiments with other techniques are needed to verify this assumption. On the other hand, the similar concentration and appearance in STM images obtained with normal tip conditions on Fe(0 0 1) with and without Mn deposition make us to identify the depressions "3" as oxygen impurities.

The effect of intermixed Fe is observed until the fourth Mn layer but decreases with layer thickness (see Fig. 4). On the fourth layer the concentration of these features equals the impurity concentration. Therefore, pure Mn layers are formed above the fourth layer. This is in agreement with the results of grazing ion-scattering measurements [16].

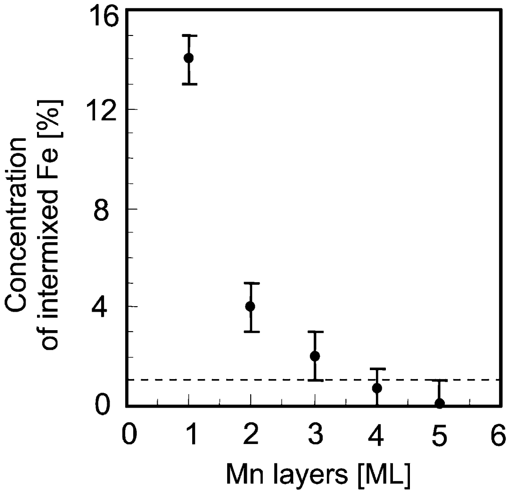

Fig. 4. The concentration of the intermixed Fe atoms in the various Mn layers. The dashed line indicates the impurity concentration.

3.3. Scanning tunneling spectroscopy

Fig. 5a shows an STM topographic image of Fe(0 0 1) covered with 1 ML Mn at a substrate temperature of 370 K. In Fig. 5a, three layers are observed: the Fe substrate layer (marked "0"), the first (marked "1a + 1b"), and the second Mn adlayer (marked "2"). Less than 1% of the substrate is still exposed. $I(V)$ curves are measured at 75 × 75 pixels at the area within the square indicated in Fig. 5a. The dI/dV map at the bias voltage of +0.8 V is shown in Fig. 5b. Based upon this dI/dV map, four kinds of dI/dV curves can be distinguished. Averages of typical 10 neighboring pixels are shown in Fig. 5c. The averaged dI/dV curve from the Fe substrate shows a peak at 0.22 eV above the Fermi energy, which is attributed to a minority spin state of d_{z^2} symmetry [38,39]. On the first Mn layer, both depressed (cf. "1a") and bright ("1b") areas can be observed in the dI/dV map (Fig. 5b). The concentration of the depressions in Fig. 5b is ~7%, [2] which corresponds to the

---

[2] Due to the high tunneling resistance ($V_S = -0.5$ V, $I = 0.5$ nA), atomic resolution cannot be obtained in the spectroscopy measurement. If one spherical depression in Fig. 5b (i.e., one marked by circle) is related to a single atom, the concentration of the depressions is roughly estimated to be ~7%.

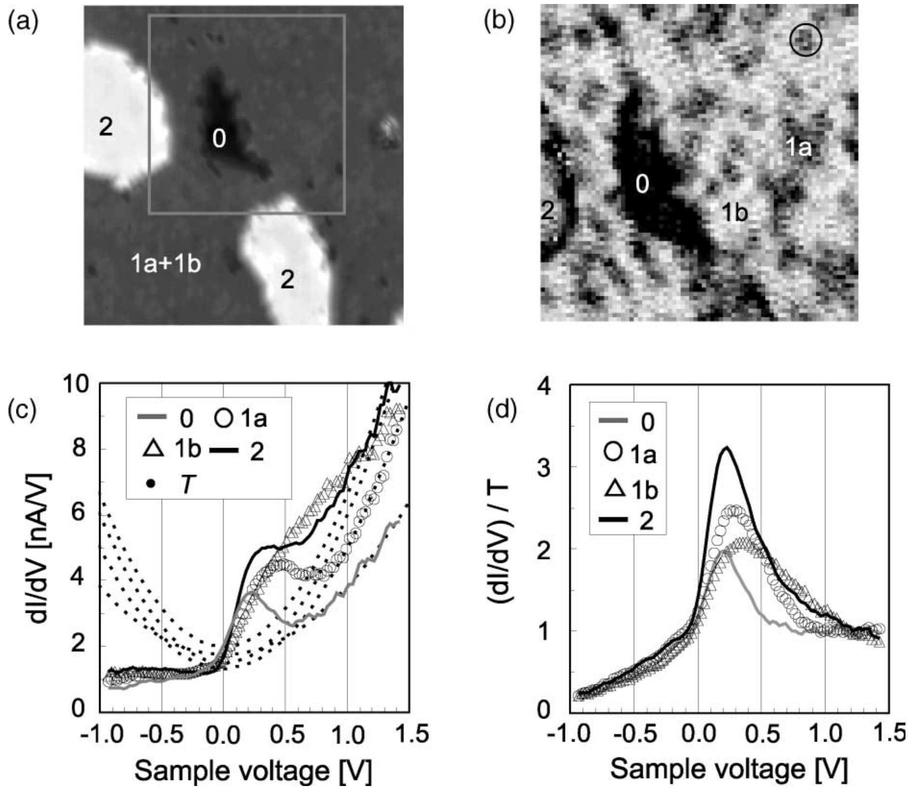

Fig. 5. STS measurement on Fe(0 0 1) covered with 1 ML Mn at 370 K: (a) is a topographic image obtained at a setpoint of $V_S = -17$ mV, $I = 0.5$ nA. Scan size is 15 × 15 nm^2. The Fe(0 0 1) surface, the first, and the second Mn layer are observed as the black (marked "0"), the grey (marked "1a + 1b"), and the white areas (marked "2"), respectively. (b) dI/dV map at +0.8 V measured at the area within the grey square in (a). Depressed (cf. "1a") and bright ("1b") areas are visible on the first Mn layer. One spherical depression is marked by a black circle. Scan size is 10 × 10 nm^2. (c) dI/dV curves representative of the areas indicated in (b). Curves are typically averages of 10 neighboring pixels. The quadratic functions fitted to the dI/dV curves are shown as dotted curves ("T"). (d) dI/dV curves of (c) normalized by quadratic background fits. Labels in (a) and (b) correspond to the ones in (c) and (d).

concentration of one kind of depressions observed in Fig. 3b. The equal concentration of the depressions implies that the depressed areas in the dI/dV map of Fig. 5b (i.e., those marked "1a") correspond to one type of Fe atoms which have been incorporated in the first Mn adlayer. The averaged dI/dV curve measured at the depressions shows a peak at 0.43 eV above the Fermi level (Fig. 5c). The averaged dI/dV curve of the bright areas "1b" does not show a peak, but it is clear that at positive voltages there is an additional contribution on top of the background (Fig. 5c). The averaged dI/dV curve obtained on the second Mn layer shows a strong shoulder around 0.3 eV above the Fermi level. The different dI/dV curves obtained on the first and the second layer must be related to the different coordination of the Mn atoms in the first and the second layer: Mn atoms in the first layer have an Fe layer underneath, while Mn atoms in the second layer cover a Mn layer.

The accurate energies of the peaks in the sample density of states (DOS) are difficult to estimate from the dI/dV curve since the apparent energies may shift due to the voltage dependence of the exponential background in the dI/dV curve [28]. Although normalization of (dI/dV) by (I/V) has been suggested as a method to remove the influence of the background, this $(dI/dV)/(I/V)$ method cannot completely remove it [40].

Ukraintsev showed that normalizing dI/dV with its fitted tunneling probability function leads to the best recovery of the sample DOS within a one dimensional WKB approach [40]. The tunneling probability function is:

$$T = a_{\mathrm{t}} \exp\left[-2S\left(\frac{2m}{\hbar^2}(\bar{\Phi} - V/2)\right)^{1/2}\right] + a_{\mathrm{s}} \exp\left[-2S\left(\frac{2m}{\hbar^2}(\bar{\Phi} + V/2)\right)^{1/2}\right].$$

The first (second) term of T describes tunneling from the tip (sample) Fermi level to unoccupied sample (tip) states. a_{t} and a_{s} are proportionality coefficients related to the tip–surface effective contact area and are proportional to the tip and the sample DOS at the Fermi level, respectively. $\bar{\Phi}$ is the average of sample and tip work functions, S the tip-sample separation, and m the electron mass. However, this recovery procedure is not very practical since it needs dI/dV data over a larger voltage range compared to usual dI/dV measurements (e.g., Fig. 5c). When there is not a large voltage range available, a fit by a quadratic function might work as well as Ref. [28] has shown. The Fe(0 0 1) dI/dV curve in Fig. 5c has been fitted on the high positive voltage side to a quadratic function. Normalizing dI/dV by this fit shifts the peak from +0.22 eV in the dI/dV curve to +0.17 eV in the normalized curve (Fig. 5d) in agreement with the reported energy of the Fe(0 0 1) surface state [39].

Using the quadratic function fit, the sample DOS of the first and second layer are recovered (Fig. 5d). By analyzing many normalized dI/dV curves, this method is believed to find the DOS peaks with an accuracy of ±0.02 eV. Although band structure calculations are needed to reveal the nature of these peaks, it seems reasonable to interpret them as Mn(0 0 1) surface states. On the first layer, the bright and depressed areas in Fig. 5b show a peak at 0.35 eV and 0.28 eV above the Fermi energy, respectively. The peak energies at the bright and depressed areas in Fig. 5b correspond to the peak energies observed on the pure Mn p(1 × 1) and the alloyed FeMn c(2 × 2) structures obtained for submonolayer Mn growth at 420 K [28]. Therefore, the bright and depressed areas in Fig. 5b can be identified as pure Mn and alloyed FeMn areas. The second layer shows a peak at 0.20 eV above the Fermi energy after normalization.

At a coverage of 2.8 ML Mn, three levels are exposed as shown in Fig. 6a. At this area, dI/dV curves were obtained at 75 × 75 pixels and averages of typically 10 curves representative of the various layers are shown in Fig. 6b. Since the dI/dV curve obtained on the lowest level of Fig. 6a is similar to the curve obtained on the second layer of Fig. 5, this level can be identified as the second Mn layer. The averaged dI/dV curve of the third Mn layer (Fig. 6b) shows a different behavior compared to the second layer. The dI/dV curve of the third layer steadily increases above the Fermi level without showing a peak or a shoulder. Whereas the averaged dI/dV curve of the fourth layer (Fig. 6b) shows a steady increase above the Fermi energy as well, the dI/dV values are lower compared to the third layer. Averaged dI/dV curves measured on films thicker than four layers are comparable to the fourth layer dI/dV curve (not shown). Fig. 6c shows the dI/dV map at +0.6 V measured at the same area as Fig. 6a. Fig. 6d shows the line profile along the white line in Fig. 6c. This line profile reveals sharp dips at the steps since the dI/dV curves measured at the steps show lower dI/dV values (Fig. 6b), which is related to a quenching of the surface states at steps [28].

For dI/dV curves measured on Mn films thicker than two layers, the quadratic function fit should also allow for an accurate evaluation of the DOS. However, the dI/dV curves show a linear-like increase up to +1.5 V. Therefore, it is impossible to fit this background to a quadratic function. For Mn films thicker than two layers, dI/dV measurements were performed within a large voltage range from −2 V to +3 V. [3] The dI/dV curves measured within this large voltage

---

[3] Although the $I(V)$ measurements at large voltages were very unstable and, frequently, some small drops ($\sim 3 \times 3 \times 0.3$ nm^3) were observed on the surface after the measurement, some reliable dI/dV curves could still be obtained.

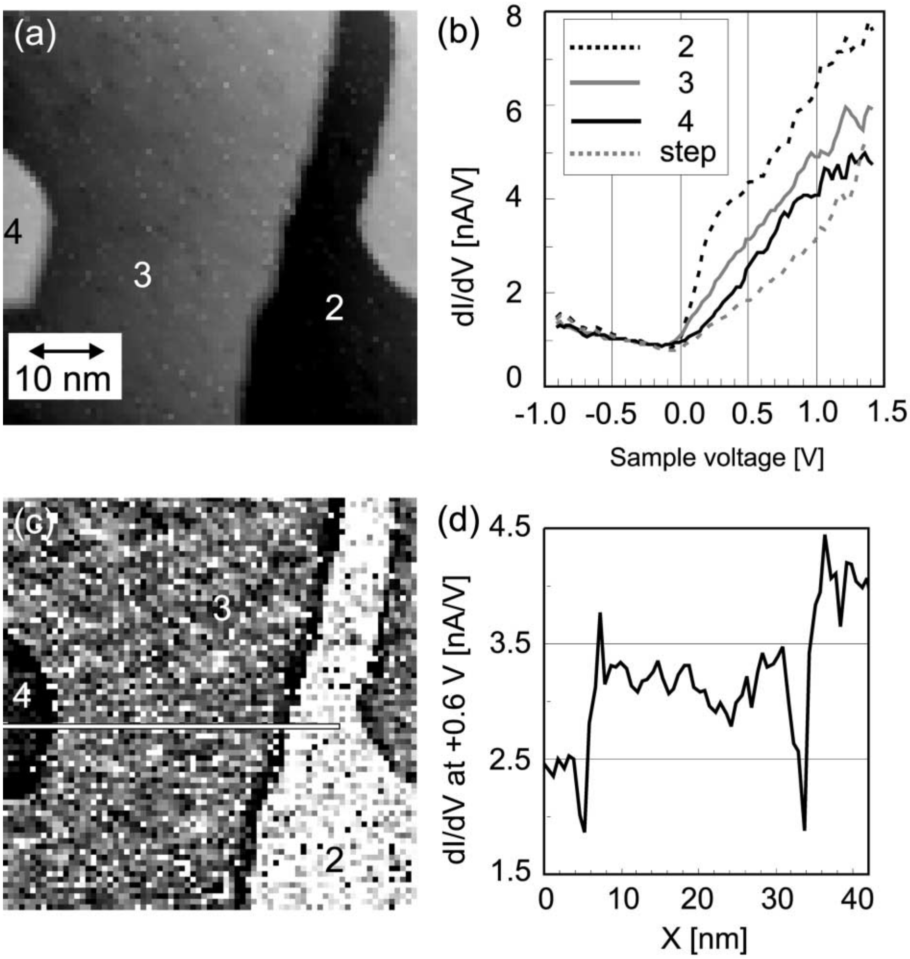

Fig. 6. STS measurement on Fe(0 0 1) covered with 2.8 ML Mn at 370 K: (a) is a topographic image obtained at a setpoint of $V_S = -0.54$ V, $I = 0.40$ nA. Scan size is 50×50 nm^2. Three different levels are exposed on the surface. (b) shows the dI/dV curves representative of each level. These curves are averages of typically 10 single curves. Since the dI/dV curve measured on the lowest level is similar to the one measured on the second layer, which is shown in Fig. 5c, this layer is identified as the second layer. (c) shows the dI/dV map at $+0.6$ V measured at the same area as (a). Numbers in (a) and (c) denote the stacking number of the Mn layers. (d) The line profile along the white line in (c) shows sharp dips at the steps.

range can be more accurately fitted by the tunneling probability function. With this normalizing technique a peak can be recovered as shown in Fig. 7. The normalized dI/dV curve measured on the third layer shows a peak around 0.8 eV above the Fermi level. For Mn films thicker than three layers, besides this $+0.8$ eV peak a weak peak at -0.6 eV is observed in $(dI/dV)/T$ curves. The $+0.8$ eV peak amplitude is about 1.3 times higher at the third layer than at thicker layers, which explains the dI/dV curves of Fig. 6b. More details about these states will be published in a forthcoming publication.

3.4. The step height

Apparent step heights were obtained from histograms of STM images. Different levels appear as

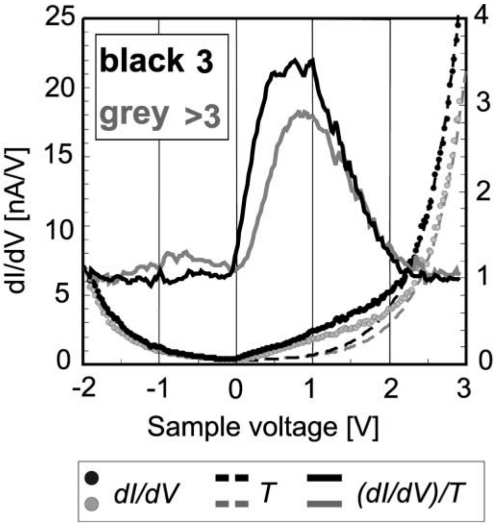

Fig. 7. dI/dV curves measured at the third layer (black dots) and layers above the third layer (grey dots). The same setpoint of $V_S = -0.5$ V, $I = 0.5$ nA was used and curves are averages of typically 20 single curves. Fits of the tunneling probability function to the dI/dV curves are also shown ("T"). The dI/dV curves normalized by this "T", i.e., "$(dI/dV)/T$", reveal a strong peak around +0.8 eV for the third Mn layer. For thicker Mn films, besides this +0.8 eV peak, a weak peak at −0.6 eV is observed in the $(dI/dV)/T$ curves as well.

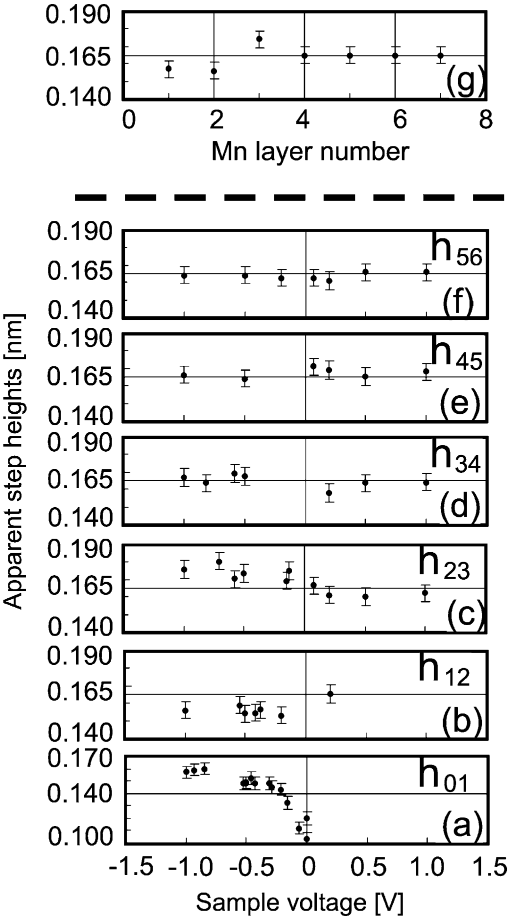

Fig. 8. Apparent step heights of the Mn layers as a function of the sample bias voltage. h_{ij} indicates the step height between level i and j. Since the heights are independent of the current, the height at each voltage is obtained from STM topographic images measured at current setpoints between 0.1 nA and 2 nA. The strong variation in h_{01} around the Fermi level is due to the Fe surface state. (g) shows the interlayer distances obtained at large negative voltages, which are believed to reflect the real geometric step heights.

sharp Gaussian peaks in this distribution with their spacings being the step heights. Only sharp Gaussian distribution profiles for which step heights unambiguously can be defined were included in the analysis.

Since variation in the apparent barrier heights may lead to different apparent step heights [41,42], apparent barrier heights were estimated from a measurement of the dependence of the tip–sample separation on the current (voltage was kept constant). However, the same apparent barrier height was obtained at each Mn layer (no tip change was observed during these measurements) and therefore this effect can be excluded.

Fig. 8 shows that the apparent step heights of the Mn layers strongly depend on the sample voltage. Since the heights are independent of the current, which was confirmed for a range from 0.1 nA to 2 nA at a constant voltage, the results of Fig. 8 are obtained from STM topographic images recorded within this current range. h_{ij} indicates the apparent step height between level i and level j. h_{01}, h_{12}, and h_{23} show a considerable voltage dependence.

Since the Fe(0 0 1) substrate layer, the first, the second, and the third Mn layer reveal peaks at different energies above the Fermi level in $(dI/dV)/T$ (see Figs. 5d and 7), h_{01}, h_{12}, and h_{23} are influenced by the electronic structure (Figs. 8a–c).

Since $(\mathrm{d}I/\mathrm{d}V)/T$ curves measured at the substrate, the first, the second, and the third layer are not completely the same at and below the Fermi level, electronic effects cannot be fully excluded from the step height measurements at large negative voltages, for which the tunneling current is dominated by sample states at the Fermi level [40]. Nevertheless, the influence of the electronic structure on the step heights is expected to be much lower at large negative voltages than at positive voltages since no strong peaks are observed at negative voltages in $(\mathrm{d}I/\mathrm{d}V)/T$. Therefore, it can be assumed that h_{01} and $h_{12} = \sim 0.16$ nm and $h_{23} = \sim 0.18$ nm give the geometric step heights. It can be concluded that: (i) The first two layers show significantly higher step heights than the Fe single step height (0.143 nm). (ii) The step height increases about 0.02 nm at the third layer compared to the first and the second layer, i.e., Mn layers on Fe(0 0 1) strongly relax at the third layer, which is in agreement with EXAFS measurements [25].

Fig. 8d shows the apparent step height between the third and the fourth layer. Whereas the scatter in h_{34} is of the same order as that in h_{45} and h_{56} (Figs. 8e and 8f), h_{34} might contain some influence of the electronic structure as well. The third layer reveals a higher amplitude of the peak at +0.8 eV compared to the fourth layer. Furthermore, the weak −0.6 eV peak present on the fourth layer is absent on the third layer (Fig. 7). In order to maintain the constant current, the tip has to move closer to the third layer at negative voltages and closer to the fourth layer at positive voltages, which qualitatively explains the variation in h_{34}. Since at both negative and positive voltages h_{34} includes electronic effects, the real geometrical step height is difficult to disentangle.

Step heights between successive Mn layers (h_{45}, h_{56}, etc) show the same values (~0.165) as shown in Figs. 8e and 8f. These step heights (h_{45} and h_{56}) are almost independent of bias voltage, which can be explained by the equal $\mathrm{d}I/\mathrm{d}V$ and $(\mathrm{d}I/\mathrm{d}V)/T$ curves measured at the fourth and higher layers. Therefore, it can be concluded that the interlayer distance for Mn films thicker than 3 ML is geometrically the same in agreement with previous results [14]. The interlayer distances between the various layers, which are obtained at large negative voltages and are believed to be the most reliable values, are shown in Fig. 8g.

4. Conclusion

Surface topographic and electronic information of Mn films grown on an Fe(0 0 1) whisker at 370 K were obtained by STM and STS at RT in UHV. Atomically and chemically resolved STM images show that the Mn film grows with the same in-plane lattice constant as Fe(0 0 1) and that Fe atoms intermix with the first, the second, and the third Mn layer. The concentration of intermixed Fe decreases with film thickness. Furthermore, STM shows that the growth mode changes from layer-by-layer to layer-plus-island at a coverage of 3 ML Mn.

$\mathrm{d}I/\mathrm{d}V$ curves normalized by voltage-dependent tunneling probability functions show peaks on each Mn layer, which can be interpreted as features in the sample DOS. The first Mn layer shows peaks at +0.35 eV on pure Mn areas and at +0.28 eV at mixed MnFe areas. The second and the third layers show peaks at +0.20 eV and +0.8 eV, respectively. Thick Mn films (>3 ML) reveal a weaker peak at −0.6 eV besides a strong peak at +0.8 eV. The +0.8 eV peak amplitude in $(\mathrm{d}I/\mathrm{d}V)/T$ curves obtained on Mn films thicker than three layers is about 1.3 times lower than that on the third Mn layer.

Based upon our apparent step height measurements, we conclude that the first two Mn overlayers show significant higher step heights than the Fe single step height and that the Mn film relaxes by about 0.02 nm at the third layer. From the fourth layer the interlayer spacings are geometrically the same (about 0.165 nm).

Acknowledgements

This work was supported by the Stichting voor Fundamenteel Onderzoek der Materie (FOM), which is funded by the Nederlandse Organisatie voor Wetenschappelijk Onderzoek (NWO), and the European Growth Project MAGNETUDE. T.K.Y. likes to thank Gakushuin University for a travel grant. We are especially grateful to B. Heinrich for supplying us with the Fe whiskers.

References

[1] H. Dreyssé, C. Demangeat, Surf. Sci. Rep. 28 (1997) 65.

[2] N. Papanikolaou, B. Nonas, S. Heinze, R. Zeller, P.H. Dederichs, Phys. Rev. B 62 (2000) 11118.

[3] B. Nonas, K. Wildberger, R. Zeller, P.H. Dederichs, Phys. Rev. Lett. 80 (1998) 4574.

[4] B. Nonas, K. Wildberger, R. Zeller, P.H. Dederichs, J. Magn. Magn. Mater. 165 (1997) 137.

[5] M. Taguchi, O. Elmouhssine, C. Demangeat, J.C. Parlebas, Phys. Rev. B 60 (1999) 6273.

[6] R. Wu, A.J. Freeman, J. Magn. Magn. Mater. 161 (1996) 89.

[7] S. Handschuh, S. Blügel, Solid State Commun. 105 (1998) 633.

[8] O. Elmouhssine, G. Moraïtis, C. Demangeat, J.C. Parledas, Phys. Rev. B 55 (1997) R7410.

[9] S. Mirbt, O. Eriksson, B. Johansson, Phys. Rev. B 52 (1995) 15070.

[10] R. Wu, A.J. Freeman, Phys. Rev. B 51 (1995) 17131.

[11] A. Vega, S. Bouarab, H. Dreyssé, C. Demangeat, Thin Solid Films 275 (1996) 103.

[12] P. Krüger, O. Elmouhssine, C. Demangeat, J.C. Parlebas, Phys. Rev. B 54 (1996) 6393.

[13] S. Bouarab, H. Nait-Laziz, M.A. Khan, C. Demangeat, H. Dreyssé, Phys. Rev. B 52 (1995) 10127.

[14] D.T. Pierce, A.D. Davies, J.A. Stroscio, D.A. Tulchinsky, J. Unguris, R.J. Celotta, J. Magn. Magn. Mater. 222 (2000) 13.

[15] R. Pfandzelter, T. Igel, H. Winter, Surf. Sci. 389 (1997) 317.

[16] T. Igel, R. Pfandzelter, H. Winter, Surf. Sci. 405 (1998) 182.

[17] D.A. Tulchinsky, D.T. Pierce, A.D. Davies, J.A. Stroscio, J. Unguris, R.J. Celotta, J. Magn. Magn. Mater. 212 (2000) 91.

[18] O. Rader, W. Gudat, D. Schmitz, C. Carbone, W. Eberhardt, Phys. Rev. B 56 (1997) 5053.

[19] Ch. Roth, Th. Kleeman, F.U. Hillebrecht, E. Kisler, Phys. Rev. B 52 (1995) R15691.

[20] T.G. Walker, H. Hopster, Phys. Rev. B 48 (1993) 3563.

[21] S. Andrieu, M. Finazzi, F. Yubero, H.M. Fischer, Ph. Arcade, F. Chevrier, L. Hennet, K. Hricovini, G. Krill, M. Piecuch, Europhys. Lett. 38 (1997) 459.

[22] J. Dresselhaus, D. Spanke, F.U. Hillebrecht, E. Kisker, Phys. Rev. B 56 (1997) 5461.

[23] S. Andrieu, M. Finazzi, F. Yubero, H. Fischer, P. Arcade, F. Chevrier, K. Hrincovini, G. Krill, M. Piecuch, J. Magn. Magn. Mater. 165 (1997) 191.

[24] S.K. Kim, Y. Tian, M. Montesano, F. Jona, P.M. Marcus, Phys. Rev. B 54 (1996) 5081.

[25] S. Andrieu, M. Finazzi, Ph. Bauer, H. Fischer, P. Lefevre, A. Traverse, K. Hricovini, G. Krill, M. Piecuch, Phys. Rev. B 57 (1998) 1985.

[26] S.T. Purcell, M.T. Johnson, N.W.E. McGee, R. Coehoorn, W. Hoving, Phys. Rev. B 45 (1992) 13064.

[27] S. Andrieu, E. Foy, H. Fischer, M. Alnot, F. Chevrier, G. Krill, M. Piecuch, Phys. Rev. B 58 (1998) 8210.

[28] M.M.J. Bischoff, T. Yamada, A.J. Quinn, H. van Kempen, Surf. Sci. 501 (2002) 155.

[29] G.J. de Raad, P.M. Koenraad, J.H. Wolter, J. Vac. Sci. Technol. B 17 (1999) 1946.

[30] S.T. Purcell, A.S. Arrott, B. Heinrich, J. Vac. Sci. Technol. B 6 (1988) 794.

[31] D.T. Pierce, J.A. Stroscio, J. Unguris, R.J. Celotta, Phys. Rev. B 49 (1994) 14564.

[32] H. Brune, K. Kern, in: D.A. King, D.P. Woodruff (Eds.), Growth and Properties of Ultrathin Epitaxial Layers, Elsevier Science, Amsterdam, 1997 (Chapter 5).

[33] E. Bauer, J.H. van der Merwe, Phys. Rev. B 33 (1986) 3657.

[34] M. Aldén, H.L. Skriver, S. Mirbt, B. Johansson, Phys. Rev. Lett. 69 (1992) 2296.

[35] M.M.J. Bischoff. PhD thesis, University of Nijmegen, The Netherlands, 2002.

[36] T. Michely, G. Comsa, J. Vac. Sci. Technol. B 9 (1991) 862.

[37] M. Schmid, W. Hebenstreit, P. Varga, S. Crampin, Phys. Rev. Lett. 76 (1996) 2298.

[38] A. Biedermann, O. Genser, W. Hebenstreit, M. Schmid, J. Redinger, R. Podloucky, P. Varga, Phys. Rev. Lett. 76 (1996) 4179.

[39] J.A. Stroscio, D.T. Pierce, A. Davies, R.J. Celotta, Phys. Rev. Lett. 75 (1995) 2960.

[40] V.A. Ukraintsev, Phys. Rev. B 53 (1996) 11176.

[41] G. Binnig, H. Rohrer, Ch. Gerber, E. Weibel, Appl. Phys. Lett. 40 (1982) 178.

[42] T. Yamada, J. Fujii, T. Mizoguchi, Surf. Sci. 479 (2001) 33.